Stabilization of G-Quadruplex DNA and Down-Regulation of Oncogene *c-myc* by Quindoline Derivatives

Tian-Miao Ou,[†,‡] Yu-Jing Lu,[†,‡] Chi Zhang,[‡] Zhi-Shu Huang,[*,‡] Xiao-Dong Wang,[‡] Jia-Heng Tan,[‡] Yuan Chen,[‡] Dik-Lung Ma,[§] Kwok-Yin Wong,[§,||] Johnny Cheuk-On Tang,[§,||] Albert Sun-Chi Chan,[§,||] and Lian-Quan Gu[*,‡]

School of Pharmaceutical Sciences, Sun Yat-sen University, Guangzhou 510080, People's Republic of China, State Key Laboratory of Chinese Medicine and Molecular Pharmacology, Shenzhen, People's Republic of China, and Department of Applied Biology and Chemical Technology and the Institute of Molecular Technology for Drug Discovery and Synthesis, The Hong Kong Polytechnic University, Hong Kong, People's Republic of China

Received August 22, 2006

Stabilization of G-quadruplex structures in the promoter region of certain oncogenes is an emerging field in anticancer drug design. Human *c-myc* gene is one of these oncogenes, and G-quadruplexes have been proven to be the transcriptional controller of this gene. In the present study, the interaction of quindoline derivatives with G-quadruplexes in *c-myc* was investigated. The experimental results indicated that these derivatives have the ability to induce/stabilize the G-quadruplexes in *c-myc*, which lead to down-regulation of the *c-myc* in the Hep G2 cell line. It was found that derivatives with terminal amino groups in their side chains would selectively bind to the isomers with the double nucleotide loops in the absence of K^+. Molecular modeling studies revealed the binding mode between the derivatives and the G-quadruplexes is end-stacking at the 3′-position, and the positively charged side chain on the quindoline derivatives may contribute to the selectivity to certain loop isomers of topological quadruplexes as well as the improved stabilization action.

1. Introduction

Human *c-myc* gene or its product is a central regulator of cellular proliferation and cell growth. The aberrant overexpression of *c-myc* is associated with a variety of malignant tumors.[1] The nuclear hypersensitivity element III_1 (NHE[a] III_1), upstream of the P1 promoter of *c-myc*, controls 80−90% of the *c-myc* transcription level.[2−6] The NHE III_1, a G (guanine)-rich strand of the DNA containing a 27 base-pair sequence, can form intramolecular G-quadruplex structures and functions as a transcriptional repressor element[7] (Figure 1). The transcription activity of *c-myc* can be inhibited by the formation/stabilization of the specific G-quadruplexes using some telomerase inhibitors, such as telomestatin,[8] TMPyP4,[9] and Se2SAP.[10] The nature product cryptolepine[11a] and its derivatives (**a**−**j**)[11b,12] have been identified by our group as telomerase inhibitors by inducing/stabilizing the G-quadruplex structure in the telomeric DNA (Figure 2). In the present study, the interactions between these quindoline derivatives and NHE III_1 DNA were investigated using polyacrylamide gel electrophoresis (PAGE), circular dichroism (CD), polymerase chain reaction stop assay (PCR stop assay), proliferation assay, reverse transcriptase PCR (RT-PCR), and molecular modeling study.

As will be shown below, our results indicated that quindoline derivatives have the ability to induce/stabilize the G-quadruplex structure in NHE III_1 DNA and inhibit the expression of *c-myc* in hepatocellular carcinoma cell line Hep G2. Quindoline derivatives with different terminal groups on their side chains were also studied to probe their selectivity toward binding of different nucleotide loop isomers. Furthermore, molecular modeling studies were also performed to understand the binding mode between the quindoline derivatives and the G-quadruplexes in *c-myc*, which might involve $\pi-\pi$ stacking and electrostatic interactions.

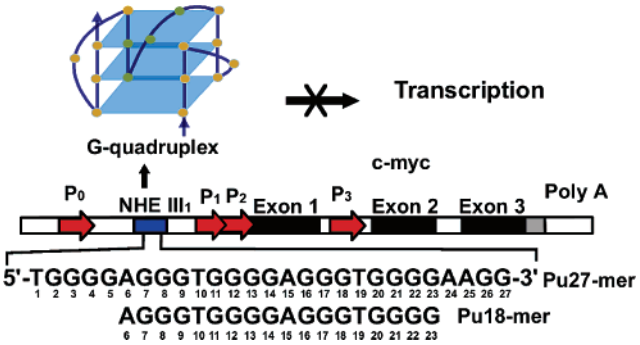

Figure 1. Location of the NHE III_1 in the *c-myc* gene and proposed biological function of G-quadruplex in this region. The numbering of the purine-rich Pu27-mer sequence and the truncated Pu18-mer are shown below. When the G-quadruplex structure formed in the promoter region of *c-myc*, the transcription will be blocked.

2. Results and Discussion

2.1 Inducing/Stabilizing the G-Quadruplex Structure in NHE III_1 by Quindoline Derivatives. PAGE was used to confirm whether the quindoline derivatives bound to the oligomer Pu27 (5′-TGGGGAGGGTGGGGAGGGTGGG-GAAGG-3′, see Figure 1) and induced/stabilized the formation of the G-quadruplex structure.[13,14] The oligomer Pu27 was incubated with derivatives **a**−**j**, respectively, for at least 4 h in a Tris-HCl buffer (10 mM, pH 7.4) or incubated with the derivatives in the presence of 100 mM KCl.

* To whom correspondence should be addressed. Phone: 8620-39332679 (Z.-S.H.); 8620-39332678 (L.-Q.G.). Fax: 8620-39332678 (Z.-S.H.); 8620-39332678(L.-Q.G.).E-mail: ceshzs@mail.sysu.edu.cn(Z.-S.H.);cedc42@zsu.edu.cn (L.-Q.G.).

† These authors contributed equally to this paper.

‡ School of Pharmaceutical Sciences, Sun Yat-sen University.

§ The Hong Kong Polytechnic University.

|| State Key Laboratory of Chinese Medicine and Molecular Pharmacology, Shenzhen.

[a] Abbreviations: G, guanine; NHE, nuclear hypersensitivity element; PAGE, polyacrylamide gel electrophoresis; CD, circular dichroism; PCR, polymerase chain reaction; RT-PCR, reverse transcriptase polymerase chain reaction; Tris, tris(hydroxymethyl)aminoethane; T_m, melting temperature; bp, base pair; IC_{50}, inhibitory concentration of 50%; DMSO, dimethyl sulfoxide; SDS, sodium dodecyl sulfate; DEPC, diethyl pyrocarbonate; BPMC, biased probability Monte Carlo.

10.1021/jm0610088 CCC: $37.00
Published on Web 03/09/2007

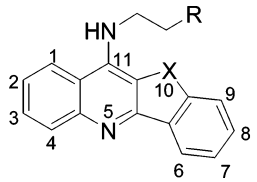

a X = NH, R = OH **b** X = O, R = OH
c X = NH, R = CH_2OH **d** X = O, R = CH_2OH
e X = NH, R = $N(CH_3)_2$ **f** X = O, R = $N(CH_3)_2$
g X = NH, R = $CH_2N(CH_3)_2$ **h** X = O, R = $CH_2N(CH_3)_2$
i X = NH, R = $N(CH_2CH_3)_2$ **j** X = O, R = $N(CH_2CH_3)_2$

Figure 2. Structures of the quindoline derivatives.

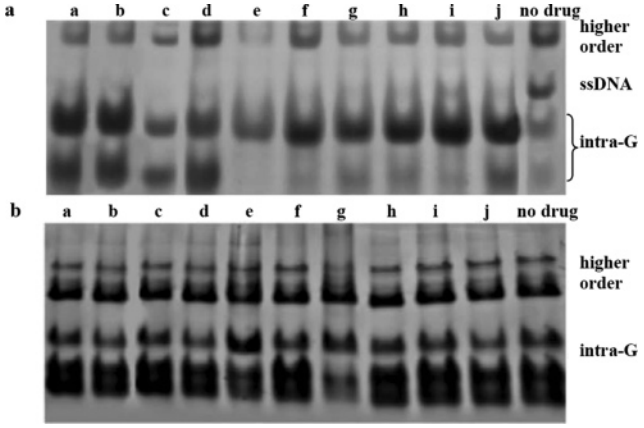

Figure 3. Polyacylamide gel electrophoresis of the oligomer Pu27 (15 μM) without (lane no drug) and with (lanes a−j) quindoline derivatives **a**−**j** (15 μM), respectively. The major bands were identified as higher order structures (higher order), single-strand structures (ss DNA), and intramolecular G-quadruplex structures (intra-G). (a) Pu27 was treated with derivatives in a Tris-HCl buffer. (b) Pu27 was treated with derivatives in a Tris-HCl buffer containing 100 mM KCl.

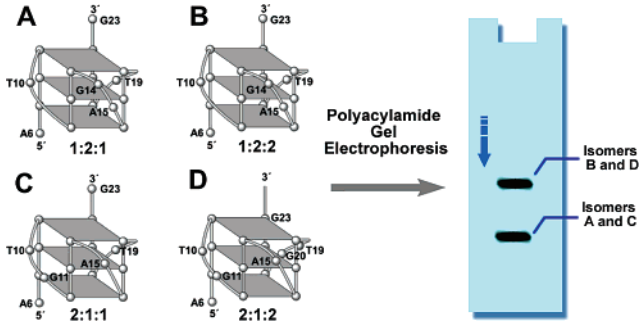

Figure 4. Proposed structures of the four different loop isomers and the corresponding proposed gel shift picture. The numbers of bases in each loop are 1:2:1, 1:2:2, 2:1:1, and 2:1:2, respectively.

According to previous gel-shift data obtained under similar experimental conditions and the mobility standards of the G-quadruplex induced by potassium ions,[4,7,10,15] the major bands were identified as higher order structures (higher order), single-strand structures (ss DNA), and intramolecular G-quadruplex structures, (intra-G; Figure 3).

All the derivatives showed interaction effects on oligomer Pu27 based on the change of mobility shift of Pu27 in the presence of the derivatives without potassium cation (Figure 3a). There appeared three major bands in the control lane (no drug) representing higher order, single strand, and intramolecular G-quadruplex structures, respectively. The former two bands were quite obvious, whereas the latter bands were less distinct (Figure 3a). In contrast, bands representing intramolecular G-quadruplex structures in lanes a−j were more distinct than the control sample (no drug), which indicated that derivatives **a**−**j** might induce the formation of two forms of intramolecular G-quadruplex.

It has been previously reported that the Pu27 oligomer could form an intramolecular quadruplex structure in the presence of 100 mM KCl.[7] In the present study, no significant difference of major bands between the treated samples and the control sample could be found after incubation in the presence of 100 mM KCl (Figure 3b), indicating that all the quindoline derivatives could not change the quadruplex structure of Pu27 induced by KCl.

It has been reported that the biologically relevant G-quadruplexes of NHE III_1 existed as a dynamic mixture of four different loop isomers A, B, C, and D, as shown in Figure 4, which had been defined through dual-mutant studies, and all four isomers contribute to the stability of the silencer element in the NHE III_1 of the *c-myc* promoter.[15] Each of the four dual-mutant Pu27 DNA could only fold into one specific loop isomer. This model study clearly demonstrated that all four loop isomeric structures existed in native Pu27 DNA. The major differences in each of the four loop isomers are the number of bases in the loops, which are 1:2:1 (A), 2:1:1 (C), 1:2:2 (B), and 2:1:2 (D), respectively (Figure 4). Among them, isomers A and C have the same total number of bases and isomers B and D have the same number of bases in loops. According to the reported data, the four loop isomers could form two bands corresponding to the intramolecular G-quadruplexes because of the different gel shift ability of the two classes of parallel loop isomers. The bottom band corresponds to isomers A and C, and the upper band corresponds to isomers B and D.[15]

It was interesting to note that the quindoline derivatives with different side chains may induce/stabilize different kinds of loop isomers in the absence of the potassium cation. The derivatives with terminal hydroxyl groups in their side chains, including **a**−**d**, showed two intra-G bands, which were almost equivalent, indicating that they might induce/stabilize all types of loop isomers. On the other hand, the derivatives with terminal amino groups in their side chains, including **e**−**j**, only induced the band with slower shift ability, which implied that they might induce only two of the loop isomers B and D. It was evident that the selective effect on loop isomers B and D by compounds **e**−**j** was not enough to change the equilibrium between the four loop isomers induced by a high concentration of the potassium cation.

2.2 Thermodynamic Stability of G-Quadruplex in the Presence of Quindoline Derivatives. The stabilization of quindoline derivatives to the G-quadruplex structure was studied by CD spectroscopy through measuring the thermodynamic stability profile of the Pu27 oligomer incubated with quindoline derivatives in the presence or absence of K^+. The change in absorption at 262 nm was monitored, which is a typical index for the parallel G-quadruplex structure in NHE III_1 DNA.[15]

The CD spectra of Pu27 incubated with derivative **f** in the absence of KCl showed a positive peak around 262 nm at room temperature, indicating that the major fraction was a parallel G-quadruplex structure. The CD spectra of Pu27 showed a diminution of this peak at high temperature, indicating the destruction of the G-quadruplex structure (Figure 5A).

Figure 5B showed the normalized CD intensity of Pu27 at 262 nm with 5 μM **f** in a Tris-HCl buffer (10 mM, pH 7.4) as a function of temperature. The melting of the native Pu27 quadruplex in 10 mM Tris-HCl occurred at 34 °C. The T_m value (53 °C) for the G-quadruplex structure of Pu27 induced by **f**

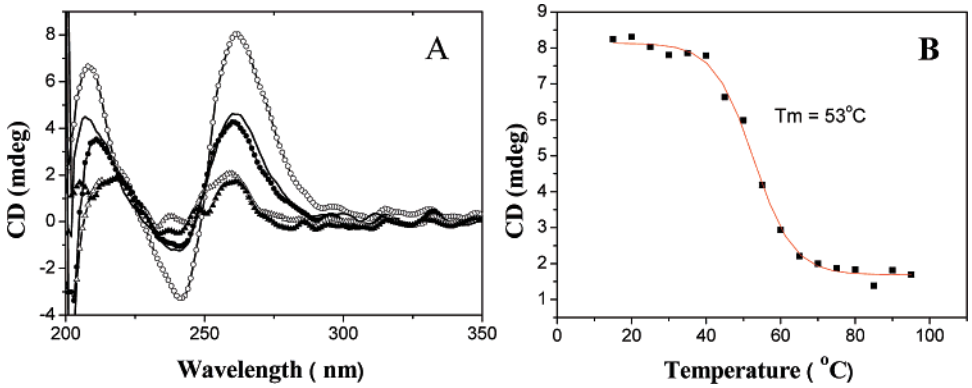

Figure 5. (A) CD spectra of Pu27 with 5 μM **f** at 25 °C (○), 55 °C (●), 75 °C (△), and 95 °C (▲) in the absence of KCl. The solid line was the spectra of Pu27 without any derivatives at 25 °C. (B) CD melting profiles of Pu27 with 5 μM **f**. All spectra were collected in a strand concentration of 5 μM in Tris-HCl buffer (10 mM, pH 7.4).

Table 1. T_m and ΔT_m of the G-quadruplex in Pu27 Induced by Derivatives **a**−**j**

derivative	T_m °C	ΔT_m °C	T_m[a] °C	derivative	T_m °C	ΔT_m °C	T_m[a] °C
no drug	34		82	**f**	53	19	>95
a	48	14	84	**g**	56	22	>95
b	47	13	85	**h**	54	20	>95
c	49	15	86	**i**	59	25	>95
d	48	14	85	**j**	55	21	>95
e	55	21	>95				

[a] T_m values of Pu27 incubated in the presence of 100 mM KCl.

was calculated from the CD melting curves at 262 nm using a sigmoidal fitting. It is clear that **f** can raise the melting temperature of the G-quadruplex by about 19 °C, indicating an obvious stabilizing effect of **f** on G-quadruplex in NHE III_1 DNA.

The changes of the T_m values of Pu27 by derivatives **a**−**j** in the absence or the presence of KCl were calculated in the same way. The T_m and ΔT_m values are summarized in Table 1. From the data obtained in the absence of KCl, derivatives **a**, **c**, **e**, **g**, and **i**, which all contain a pyrrole ring, showed a comparatively higher T_m value versus derivatives **b**, **d**, **f**, **h**, and **j**, which contain a furan ring. This indicated that the relatively strong electron-donating of the nitrogen in the pyrrole ring contribute positively to the binding affinity with G-quadruplex DNA. More interestingly, the structural difference in the side chains showed significantly different effects on the binding affinity with G-quadruplex DNA. According to the T_m value, derivatives **a**−**d**, with side chains containing the terminal hydroxyl group, showed a comparatively lower T_m value versus derivatives **e**−**j**, which had terminal amino groups in their side chains. It is clear that the derivatives containing a pyrrole ring and an amino group side chain demonstrated higher binding affinity with G-quadruplex DNA, resulting in an increase in the $\pi-\pi$ stacking ability of the core and the positive charges in the side chain.

All the T_m values of Pu27 incubated with the derivatives in the presence of 100 mM KCl showed an increase of at least 2 °C when compared to the T_m value of 82 °C for Pu27 in the presence of 100 mM KCl, indicating that the derivatives could increase the stabilization of the quadruplex structures of Pu27 induced by KCl, although they could not increase the percentage of the quadruplexes, as shown in Figure 3b.

2.3 Inhibition of Amplification in the Promoter Region of *c-myc* by Quindoline Derivatives. The induction of biologically relevant G-quadruplex formation in Pu27 by quindoline derivatives was investigated using PCR stop assay. The specific binding of ligands with intramolecular G-quadruplex structures

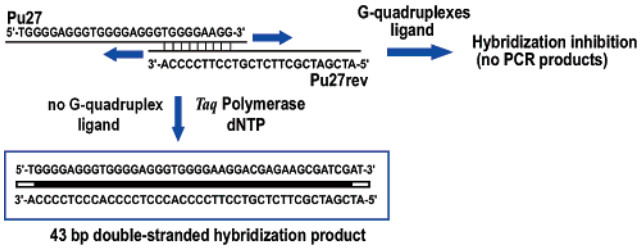

Figure 6. Principle of the PCR stop assay. Test oligomer was amplified with a complementary oligomer overlapping the last G-repeat. *Taq* polymerase extension resulted in the formation of a final 43 base pair (bp) double-stranded PCR product. In the presence of a ligand that stabilizes test oligomers into a G-quadruplex structure, annealing of oligomer and, therefore, *Taq* polymerase extension was inhibited. Underlined sequence corresponds to overlap between the two oligomers.

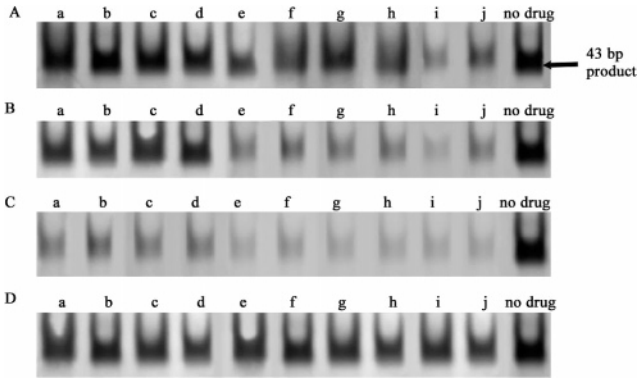

Figure 7. Effects of quindoline derivatives **a**−**j** on the PCR-stop assay with G-quadruplex forming Pu27 oligomer. Different derivatives with a certain concentration at 6 μM (A), 18 μM (B), and 36 μM (C) were added to Pu27 oligomer, as indicated according to the Experimental Section. The band (arrow) presented the 43 bp double-stranded PCR product. Parallel experiments were performed using all these derivatives in oligomer Pu27-13,14 at a concentration of 36 μM, shown in D.

in the promoter region could inhibit the action of the DNA polymerase.[16] In the presence of the derivatives, the single strand Pu27 was induced into a G-quadruplex structure that blocked hybridization with a complementary strand overlapping the last G repeat (Figure 6). In that case, the 5′ to 3′ extension with *Taq* polymerase was inhibited, and the final double-stranded DNA PCR product could not be detected.[8]

Different concentrations of derivatives at 6, 18, and 36 μM were used in this assay. Derivative **i** showed an inhibitory effect on the hybridization of oligomer Pu27 and Pu27rev when the derivative concentration was 6 μM (Figure 7A). Other derivatives with terminal amino groups in their side chains, including

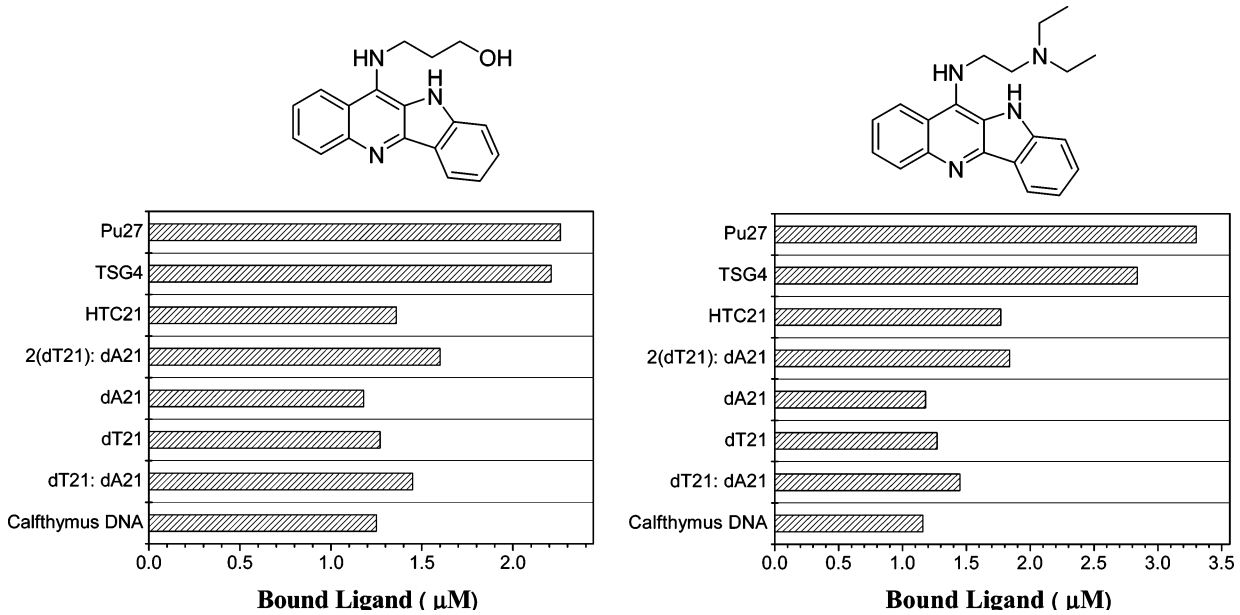

Figure 8. Results of competition dialysis experiment. A 1 μM solution of **c** or **i** was dialyzed against eight different nucleic acid structures (40 μM) for 24 h. The amount of **c** or **i** bound to each structure was plotted as a bar graph. The structures of these two derivatives were also shown above the bar graph, respectively. Left, bar graph and structure of derivative **c**; right, bar graph structure of derivative **i**.

derivatives **e**, **f**, **g**, **h**, and **j** showed an inhibitory effect on the hybridization when the derivative concentration was increased to 18 μM (Figure 7B). Furthermore, derivatives having a terminal hydroxyl group in their side chain, including derivatives **a**−**d**, showed a weaker inhibitory effect on the hybridization and inhibited the hybridization only at a higher concentration of 36 μM (Figure 7C). These results were correlated to the T_m values in Table 1, which indicated that the stability of G-quadruplexes induced by quindoline derivatives is an important factor for inhibiting the gene expression.

To further demonstrate the inhibitory effects of quindoline derivatives against the G-quadruplex stabilization of Pu27, a parallel experiment using an oligomer Pu27-13,14 (5′-TGGG-GAGGGT-GGAAAGGGTGGGGAAGG-3′), which could not form the G-quadruplex structure was performed. Under such circumstances, no inhibition was observed even at the highest concentration of 36 μM (Figure 7D).

2.4 Competition Dialysis. To evaluate the selectivity of quindoline derivatives for G-quadruplex and other DNA structures, we performed a competitive dialysis experiment using different types of DNA. Among the DNA used in the present study, Pu27 and TSG4 could form the G-quadruplex structures, HTC 21 could form the i-motif structure, $(dT21)_2$/dA21 was associated to a triplex structure, dT21/dA21 was associated to a duplex structure, dA21 and dT21 were single-strand purine and pyridine structures, respectively, and calf thymus DNA was a native duplex DNA structure. Higher binding affinity was reflected by the higher concentration of ligands accumulated in the dialysis cassette containing the specific form of DNA.[17]

The data in Figure 8 were shown as bar charts in which the amount of bound ligand was plotted for eight structurally different nucleic acids. In this assay, the various nucleic acids were dialyzed simultaneously against a free ligand solution. The amount of bound ligand was directly proportional to the binding constant for each conformer of DNA. As shown in Figure 8, the amount of bound ligand in derivative **c** did not vary significantly for different types of DNA, whereas derivative **i** interacted preferentially with G-quadruplex DNA in Pu27 and TSG4. These indicated that derivative **i** has a better selectivity for G-quadruplex DNA, especially for those in Pu27, than derivative **c**.

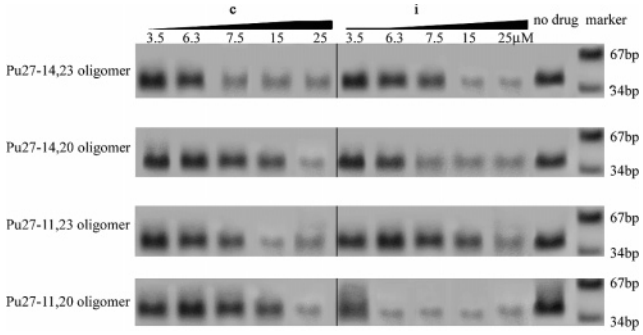

Figure 9. Effects of quindoline derivatives **c** and **i** on the PCR-stop assay with four mutant Pu27 oligomers. The two derivatives with a certain concentration at 3.5, 6.3, 7.5, 15, and 25 μM were added to different mutant oligomers of Pu27, as indicated according to the Experimental Section. The band presented the 43 bp double-stranded PCR product. Parallel experiments were performed in the oligomers without drug treatment.

2.5 Selectivity for Binding Loop Isomers of G-Quadruplex by Quindoline Derivatives of Different Structures. Four mutant oligomers were used for the PCR stop assay, including oligomer Pu27-14,23 forming isomer A, Pu27-11,23 forming isomer C, Pu27-14,20 forming isomer B, and Pu27-11,20 forming isomer D (Figure 4).[15] Two derivatives, **c** and **i**, were chosen for studying their effects on inducing/stabilizing different parallel loop isomers of G-quadrulex. A decrease in PCR products associated with the interaction between quindoline derivatives and mutant oligomers occurred. The decrease in PCR products were observed after the isomers had been incubated with derivatives **c** or **i** at specific concentration, but interestingly, the two derivatives showed different inhibitory behaviors on each of the four loop isomers (Figure 9). The minimum concentration of derivative **i** for effective interaction with oligomer Pu27-14,20 and Pu27-11,20 was significantly lower than that for oligomer Pu27-14,23 and Pu27-11,23. On the other hand, the interaction concentrations of **c** were relatively higher

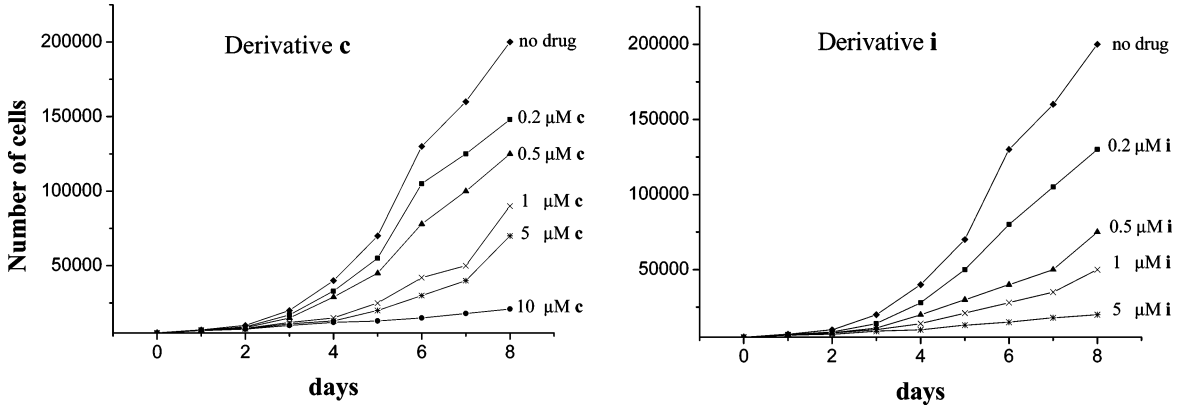

Figure 10. Effect of derivatives **c** or **i** on cell proliferation. In vitro growth curves of the Hep G2 hepatocellular carcinoma cells untreated (◆) and treated with 0.2 (■), 0.5 (▲), 1 (×), 5 (∗), and 10 (●) μM of derivatives **c** or **i**. The derivatives were added to the culture medium at days 1 and 5 of culture.

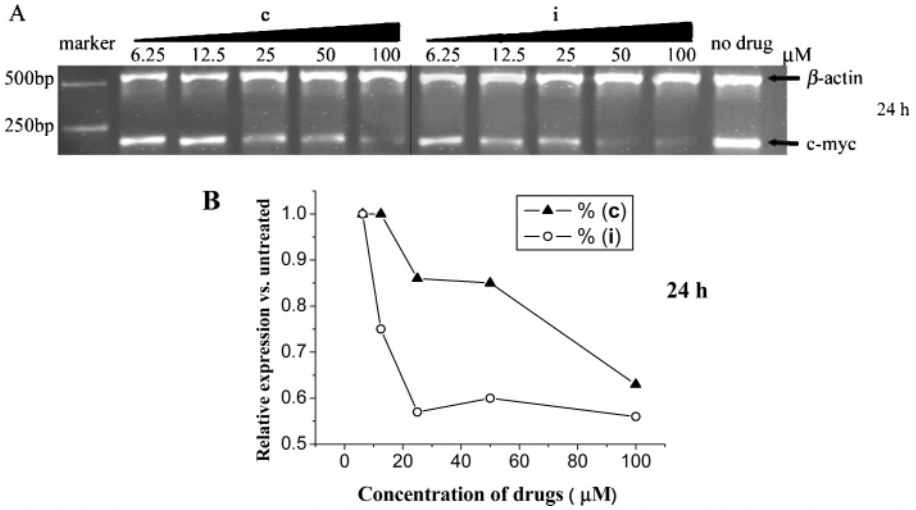

Figure 11. RT-PCR to determine the expression of *c-myc* in the HepG2 cell line treated with derivatives **c** and **i**. (A) 5×10^5 Hep G2 cells were treated in a 25-cm^2 flask with medium (no drug), 6.25, 12.5, 25, 50, and 100 μM of derivative **c** or **i** for 24 h, and the total RNA was extracted and subjected to reverse transcription, followed by PCR for *c-myc* and *β-actin* (control). Amplified products were 191bp for *c-myc* and 541bp for *β-actin*. (B) The optical density of each band by using Quantity One software (Biorad). The graph showed the relative expression of *c-myc* as compared with the "no drug" sample for each time point versus concentration of the derivative **c** (▲) and **i** (○).

and did not show distinct difference in the four mutant oligomers. The results indicated that derivative **i** bound selectively to isomers B and D, and **c** could not show a distinct selectivity of the four isomers.

The selectivity of quindoline derivatives to certain G-quadruplex isomers may be correlated with the interaction pattern between the derivatives and the loop isomers. There were two types of interactions involved in the binding of ligands to G-quadruplexes: a stacking-type interaction between the quindoline core and the G-tetrad guanines and an electrostatic interaction between the positive charges of ligand and the negative charges of phosphate backbone of DNA. As reported, the G-tetrad arrangement and the orientation of the loops are important factors for the interaction,[10] and the electrostatic interactions between the ligand side chains and the DNA phosphates play a significant role in selecting its topology.[18a,b] As electrostatic interaction between the quindoline derivatives and the DNA contributes strongly to the inducing/stabilizing ability, the orientation difference of the loops in the isomers could result in the selectivity of quindoline derivatives.

2.6 Inhibition of the Expression of *c-myc* in the Cancer Cell Line. To evaluate the inhibitory abilities of derivatives on the expression of *c-myc* in the cancer cell line, proliferation assays were carried first. Figure 10 showed the cell viability of hepatocellular carcinoma cell line Hep G2 treated with derivatives **c** or **i** of increasing concentrations, ranging from 0.2 to 10 μM. A decrease of cell proliferation was found on day 2 after treatment, and a dose-dependent decrease of cell proliferation was evident after treatment with both derivatives on day 3. In five-day growth inhibition assays, the IC_{50} value of derivative **c** was ~1 μM and **i** was ~0.2 μM. In seven-day growth inhibition assays, the IC_{50} value of derivative **c** was ~1.3 μM and **i** was ~0.3 μM. According to these data, the treated concentrations of expression assay were chosen as 6.25, 12.5, 25, 50, and 100 μM to minimize the cell toxicity effect of the derivatives.

For the expression assay of *c-myc* in cancer cell lines, about 5×10^5 Hep G2 cells were seeded into six-well plates, incubated for 1 day, and then treated with derivative **c** or **i** at 6.25, 12.5, 25, 50, and 100 μM for 24 h. The total RNA was extracted and reverse transcripted to cDNA. This cDNA was then used as a template for specific PCR amplification of the *c-myc* sequence and controlled by *β-actin*.

The decreasing/disappearing of *c-myc* PCR products was significant when treated with either derivative **c** or derivative **i** (Figure 11). As shown in Figure 11B, 12.5 μM of derivative **i** started to inhibit the expression of *c-myc* and total inhibitory behavior was observed at 50 μM, while 25 μM of **c** started to

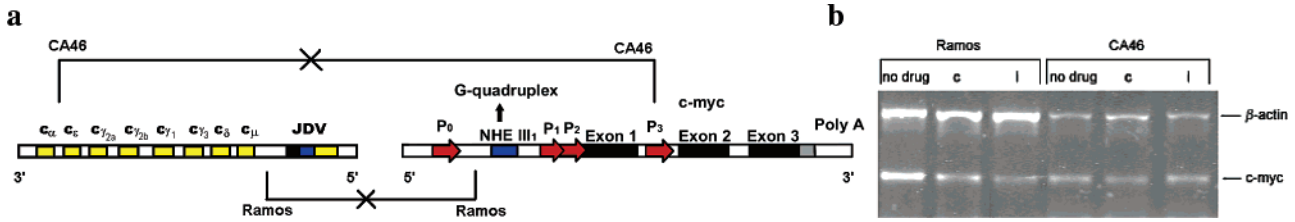

Figure 12. Effect of the quindoline derivatives **c** and **i** on *c-myc* expression in two different Burkitt's lymphoma cell lines. (a) Diagram of the rearrangements involved in the Ramos and CA46 Burkitt's lymphoma cell lines. (b) RT-PCR for *c-myc* and *β-actin* in Ramos (lanes 1−3) and CA46 (lanes 4−6) cell lines after no treatment (lanes 1 and 4) and after treatment with 10 μM of derivatives **c** (lanes 2 and 5) and **i** (lanes 3 and 6) for 24 h.

inhibit, and the total inhibitory behavior of **c** was observed at 100 μM. The results were consistent with the results in the PCR stop assay.

To further confirm that the derivatives targeted the quadrulex structures in the promoter region of *c-myc* and hence produced the inhibition of the expression of *c-myc*, two Burkitt's lymphoma cell lines with different translocation break points within the *c-myc* were tested. The Ramos cell line retains the NHE III_1 during translocation, which the CA46 cell line has lost this element together with the P1 and P2 promoters (Figure 12a).[19,20] With the NHE III_1 element deleted, as in the CA46 cell line, both derivatives **c** and **i** showed no effect on *c-myc* expression, whereas in the Ramos cell line, which retained this element, both derivatives could lower the *c-myc* expression, and a difference in inhibition on *c-myc* expression by derivatives **c** and **i** was observed.

2.7 Molecular Modeling Study on Interactions between Quindoline Derivatives and G-Quadruplex Structures in the NHE III_1. To further investigate the binding modes and selectivity between the quindoline derivatives and the intramolecular G-quadruplex loop isomers of NHE III_1, molecular modeling methods including molecular dynamics and docking simulations were performed. As previous reports indicated that nucleotides G2−G5 in the Pu27-mer were not involved in the G-quadruplex structure,[7] the truncated sequence Pu18-mer (A6-G23 in Pu27-mer, Figure 1) was used for subsequent studies. Job plot[21] with the oligomer Pu27 showed a stoichiometry of one quindoline derivative (**c** or **i**) bound per quadruplex (See Figure SI-18 of Supporting Information). Models of two possible loop isomers of Pu18 parallel G-quadruplex, namely, isomers A and B (Figure 4), were built. The main difference between isomer A and isomer B was the number of bases in their loops. Isomer A adopted a loop pattern of 1:2:1, while isomer B had one more double-nucleotide loop and adopted a loop pattern of 1:2:2.

After molecular dynamics simulations, the parallel G-quadruplex structures A and B were found to be stable and did not undergo major conformational rearrangements. The G-tetrads were found to be relatively stable through the course of simulations, but the position of loop nucleotides changed significantly and exhibited more variance. Single-nucleotide side loops and double-nucleotide side loops behaved differently in both of the loop isomers. The strong tension of backbone atoms in single-nucleotide side loops decrease the flexibility of the loop, while in the double-nucleotide loops, the backbone atoms had fairly good flexibility. Distance analysis on G-tetrads showed that the hydrogen bonds remained stable, but tension from single-nucleotide side loops slightly influenced their planarity and made the neighboring tetrad nucleotides relatively unstable. The global minimum conformations of isomers A and B were extracted from the trajectory records of molecular dynamics simulations. After further refinement, these structures

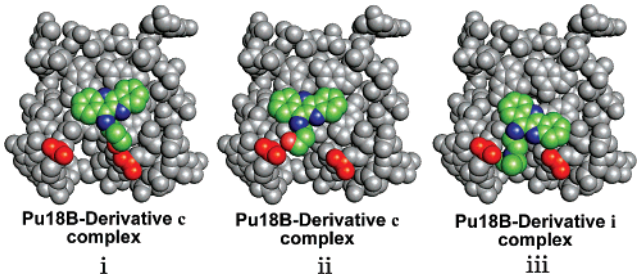

Figure 13. View onto the plane of the 3′ surface of Pu18 G-quadruplex, showing the interactions between quindoline derivatives and G-quadruplex. For clarity, hydrogen atoms and potassium ions are removed, and the phosphate diester backbone atoms in G-quadruplex and loop nucleotides in the binding side are colored in red. Pictures were created with PyMOL.[25]

were used as initial models to perform molecular docking simulations and study their interactions with quindoline derivatives.

Derivatives **c** and **i** were docked into the modeled structure of isomers A and B, respectively, utilizing the ICM program (Molsoft).[22] Binding modes of these complexes were found to be consistent, and both of the derivatives preferred stacking on the exterior 3′ surface of G-quadruplex. The chromphore moieties of the derivatives could form aromatic $\pi-\pi$ stacking interactions with G-tetrads, while the positive center of 5-N placed over the highly negative charged central carbonyl channel and formed strong electrostatic interactions. Side chain oxygen atoms and nitrogen atoms were able to form hydrogen bonds with phosphate diester backbone. This also explains why the 3′ surface, which favors electrostatic interactions[23] and has more exposed phosphate diester atoms,[24] is more favorable for binding.

Cluster analysis of the docking result of ligand−DNA complexes showed that there were two major binding conformations distinguished by the direction of the side chain. As illustrated in Figure 10, the side chain hydroxyl or amino group can form a hydrogen bond with the phosphate diester backbone in either the G-quadruplex (**i** in Figure 13) or the loop nucleotide (**ii** and **iii** in Figure 13). It is worthy to note that the hydroxyl or amino group on the side chain of the quindoline derivative, when interacting with a loop nucleotide, could only reach the phosphate backbone atoms in double-nucleotide loops (**ii** and **iii** in Figure 13). In single-nucleotide loops, the phosphate backbone atoms were away from the center of the G-tetrad and directions were unfavorable for binding (Figure 14). Moreover, the lack of flexibility of single-nucleotide loops made changing of this unfavorable conformation relatively difficult. In this way, the different action of double-nucleotide loops and single-nucleotide loops with the ligands' side chain may lead to the selectivity on different isomers of quindoline derivatives. These findings are in accord with a previous study on the solution structure of the biologically relevant G-quadruplex in *c-myc*

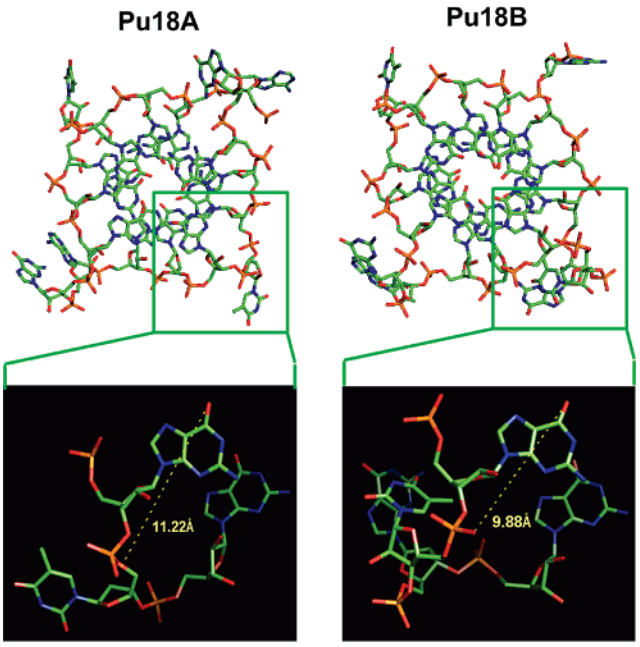

Figure 14. Structure of a single-nucleotide loop (left) taken from the modeled structure of Pu18 isomer A and a double-nucleotide loop (right) taken from the modeled structure of Pu18 isomer B. The distance between the central carbonyl channel and the phosphate diester atoms in the loop nucleotide was measured. Pictures were created with PyMOL.[25]

promoter[26] and suggest that isomers with more double-nucleotide loops (isomers B and D) will favor binding to the side chains of quindoline derivatives. However, derivative **c** did not show selectivity on loop isomers based on our experimental results, because the hydrogen bond interaction between the side chain hydroxyl group and the phosphate diester backbone has only a minor contribution to the binding compared to the strong electrostatic and aromatic interactions between the quindoline scaffold and the G-quadruplex. Thus, the small influence of the side chain hydroxyl group on the selectivity of loop isomers could not be detected in the aforementioned experiments. For derivative **i**, with stronger interactions between the side chain and the phosphate diester backbone, it did show a good selectivity on isomers B and D. Compound **i** exhibits the highest binding interaction (as measured by the binding energy of −56.66 kcal/mol) toward Pu18B, it is end-stacked at the 3′ of the G-quadruplex DNA. This finding is consistent with the proposed specificity from the PAGE and PCR stop assay. Furthermore, the unfavorable binding energies of 30−140 kcal/mol suggested that the interactions between these two quindoline derivatives and G-quadruplex DNA should not be intercalative in nature (Table 2).

3. Conclusion

In summary, a series of quindoline derivatives have been investigated on their interactions with G-quadruplexes in *c-myc*. It was found that derivatives with different structures had different abilities to induce/stabilize the G-quadruplexes in *c-myc*, leading to a different degree of inhibition on the *c-myc* gene in the hepatocellular carcinoma cell line. Furthermore, derivatives with an amino group on the side chain would selectively interact with the longer loop isomers (isomers B and D in Figure 4) in the absence of the potassium cation, and the selectivity of the interaction was suppressed in the presence of the potassium cation. It could be inferred that the binding of the compounds to the less stable isomers B and D was not strong enough to change the equilibrium between the four loop isomers, as a previous study indicated that the shorter loop isomers (isomers A and C in Figure 4) were more thermodynamically stable.[15] Molecular modeling studies revealed that the presence of an amino group in the side chain could strengthen the electrostatic interaction between the derivatives and the phosphate backbone and hence contribute to the inducing/stabilizing effect on G-quadruplexes and the selectivity toward certain loop isomers of G-quadruplexes.

Table 2. Calculated Binding Energies (in kcal/mol) for Derivatives **c** and **i** Bound to Different Binding Sites of the Pu18 G-Quadruplex Loop Isomers A and B

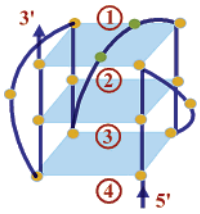

	binding energy (kcal/mol)			
complex	end stacking at 3′ ①[a]	intercalation near 3′ ②[a]	intercalation near 5′ ③[a]	end stacking at 5′ ④[a]
Pu18A−**i**	−44.84	56.23	126.62	−39.21
Pu18A−**c**	−43.00	30.39	54.15	−39.63
Pu18B−**i**	−56.66	140.80	88.93	−41.85
Pu18B−**c**	−44.96	55.43	62.17	−40.74

[a] Binding sites.

4. Experimental Section

Materials. All oligomers/primers used in this study were purchased from Invitrogen (China), and their sequences were listed in Table 3. Acrylamide/bisacrylamide solution and *N,N,N′,N′*-tetramethyl-ethylenediamine were purchased from Sigma. *Taq* DNA polymerase was purchased from Sangon, China. The total RNA isolation kit and the two-step RT-PCR kit were purchased from SBS Genetech, China. All the derivatives were synthesized as previously reported.[11] Stock solutions of all the derivatives (10 mM) were made using DMSO (10%) or double-distilled water. Further dilutions to working concentrations were made with double-distilled water.

Polyacrylamide Gel Electrophoresis. The oligomer Pu27 at a final concentration of 10 μM was heated to 95 °C for 10 min in Tris-HCl buffer (10 mM, pH 7.4). After the solution was gradually cooled to room temperature, a 1 μL stock solution of the derivatives was added to each sample to produce the specified concentrations at a total volume of 10 μL. The reaction mixture was incubated overnight at 4 °C. After incubation, 2 μL of loading buffer (50% glycerol, 0.25% bromophenol blue, and 0.25% xylene cyanol) was added to each mixture. Ten micro liter aliquots of each sample were subsequently analyzed by native 15% PAGE. The gels were silver-stained and photos were taken. The same assays were repeated as above in a Tris-HCl buffer (10 mM, pH 7.4) containing 100 mM KCl.

Circular Dichroism. The oligomer Pu27 at a final concentration of 5 μM was resuspended in Tris-HCl buffer (10 mM, pH 7.4) containing the derivatives to be tested. The samples were heated to 95 °C, then gradually cooled to room temperature, and incubated at 4 °C for at least 6 h. The CD spectra were recorded on a Jasco J-810 spectropolarimeter, using 16 scans at 100 nm/min, a 1 s response time, and a 1 nm bandwidth. The CD spectra were obtained by taking the average of two scans made from 200 to 400 nm. In the melting studies, the temperature of the sample was maintained by a Jasco Pelter temperature controller. The melting curves of the G-quadruplex were measured with the intensity at 262 nm. Before the CD spectroscopy, all the samples were thermally treated as described above. The same assays were repeated as above in a Tris-HCl buffer (10 mM, pH 7.4) containing 100 mM KCl.

Table 3. Sequences of Oligomers (Primers) Used in the Present Study

name of oligomer	sequence	description
Pu27	5′-TGGGGAGGGTGGGGAGGGTGGGGAAGG-3′	Partial sequence in the promoter of oncogene *c-myc* that may form G-quadruplex.
Pu27-11,20	5′-TGGGGAGGGTTGGGAGGGTTGGGAAGG-3′	Dual mutant of Pu27, whose mutant sites were 11 and 20.
Pu27-11,23	5′-TGGGGAGGGTTGGGAGGGTGGGTAAGG-3′	Dual mutant of Pu27, whose mutant sites were 11 and 23.
Pu27-14,20	5′-TGGGGAGGGTGGGTAGGGTTGGGAAGG-3′	Dual mutant of Pu27, whose mutant sites were 14 and 20.
Pu27-14,23	5′-TGGGGAGGGTGGGTAGGGTGGGTAAGG-3′	Dual mutant of Pu27, whose mutant sites were 14 and 23.
Pu27-13,14	5′-TGGGGAGGGTGGAAAGGGTGGGGAAGG-3′	Mutant oligomer of Pu27 that may not form G-quadruplex, whose mutant sites were 13 and 14.
Pu27rev	5′-ATCGATCGC TTCTCGTCCTTCCCCA-3′	Complementary sequence of Pu27 in PCR stop assay.
Pu27rev-2	5′-ATCGATCGC TTCTCGTCCTTACCCA-3′	Complementary sequence of Pu27-11,23 and Pu27-14,23 in PCR stop assay.
Pu27rev-3	5′-ATCGATCGC TTCTCGTCCTTCCCAA-3′	Complementary sequence of Pu27-11,20 and Pu27-14,20 in PCR stop assay.
TSG4	5′-GGGTTAGGGTTAGGGTTAGGG-3′	Partial sequence in human telomere that may form the G-quadruplex structure.
HTC21	5′-CCTAACCCTAACCCTAACCC-3′	Complementary sequence of TSG4 that may form an i-motif structure.
Pu18	5′-AGGGTGGGGAGGGTGGGG-3′	Truncated sequence of Pu27 that involved in the G-quadruplex forming.
c-myc A	5′-TGGTGCTCCATGAGGAGACA-3′	Upstream primer for *c-myc* in RT-PCR[27].
c-myc S	5′-GTGGCACCTCTTGAGGACCT-3′	Downstream primer for *c-myc* in RT-PCR.
β-actin A	5′-GTTGCTATCCAGGCTGTGC-3′	Upstream primer for *β-actin* as control in RT-PCR[27].
β-actin S	5′-GCATCCTGTCGGCAATGC-3′	Downstream primer for *β-actin* as control in RT−PCR.

Table 4. Nucleic Acid Conformation and Samples Used in Competition Dialysis Experiments

conformation	DNA/oligonucleotide	ϵ ($M^{-1}\cdot cm^{-1}$)
single strand purine	dA21	255 400
single strand pyriminde	dT21	170 700
duplex DNA	calf thymus (42% GC)	12 824
	dT21/dA21	12 000
triplex DNA	$(dT21)_2$/dA21	17 200
quadruplex DNA	Pu27 (5′-TGGGGAGGGTGGGGAGGGTGGGGAAGG-3′)	223 920
	TSG4 (5′-GGGTTAGGGTTAGGGTTAGGG-3′)	172 000
i-motif	HTC21 (5′-CCCTAACCCTAACCCTAACCC-3′)	148 720

PCR Stop Assay. The PCR stop assay was performed with a modified protocol of the previous study.[8] Sequences of the test oligomers, including Pu27, Pu27-13,14, Pu27-11,20, Pu27-11,23, Pu27-14,20, and Pu27-14,23, and the corresponding complementary sequence used in the current study were presented in Table 3. The reactions were performed in 1×PCR buffer, containing 10 μmol of each pair of oligomers, 0.16 mM dNTP, 2.5 U *Taq* polymerase, and the indicated amount of the derivatives in Figures 6 and 8. Reaction mixtures were incubated in a thermocycler, with the following cycling conditions: 94 °C for 3 min, followed by 30 cycles of 94 °C for 30 s, 58 °C for 30 s, and 72 °C for 30 s. Amplified products were resolved on 15% nondenaturing polyacrylamide gels in 1×TBE and silver stained.

Competition Dialysis Assay. A Tris-HCl buffer (10 mM, pH 7.4) containing 100 mM NaCl was used for all experiments. Derivatives **c** and **i** were respectively used in this assay. For each competition dialysis assay, 400 mL of dialysate solution containing 1 μM derivative was placed into a beaker. A volume of 0.5 mL (at 40 μM monomeric unit) of each of the DNA samples was pipeted into a separate 0.5 mL Spectro/Por DispoDialyzer unit with a 1000 molecular weight cutoff tubing (Spectrum, Laguna Hills, California). A panel of eight different nucleic acid structures used was listed in Table 4. The entire dialysis units were then placed in the beaker containing the dialysate solution. The contents were allowed to equilibrate with continuous stirring for 24 h at room temperature. At the end of the equilibration, DNA samples were carefully removed to microfuge tubes and were taken to a final concentration of 1% (w/v) sodium dodecyl sulfate (SDS). The total concentration of derivative (C_t) within each dialysis cassette was then determined spectrophotometrically using a wavelength of 413.6 nm and an extinction coefficient of 10 210 $M^{-1}\cdot cm^{-1}$ for derivative **c** and a wavelength of 414.8 nm and an extinction coefficient of 11 420 $M^{-1}\cdot cm^{-1}$ for **i**. The free ligand concentration (C_f) was determined spectrophotometrically using an aliquot of the dialysate solution. The amount of bound ligand was determined by the difference between the total ligand concentration and the free ligand concentration ($C_b = C_t - C_f$).

Cell Culture. The hepatocellular carcinoma cell line Hep G2 and the Burkitt's lymphoma cell lines, Ramos and CA46, were obtained from the American Type Culture Collection (ATCC; Rockville, MD). The cells cultures were maintained in RPMI-1640 medium supplemented with 10% fetal bovine serum, 100 U/mL penicillin, and 100 μg/mL streptomycin in 25 cm^2 culture flasks at 37 °C humidified atmosphere with 5% CO_2.

Proliferation Assay. For the proliferation assay, about 5000 Hep G2 cells were seeded in a 24-well microplate, and at 24 h after plating, increasing concentrations of freshly dissolved compound **c** or **i**, ranging from 0.2 μM to 10 μM, were added to the culture medium, which were then left for 4 days. Then, at day 5, the compounds were re-added to medium and left for an additional 4 days. Cell counts and viability (trypan blue dye exclusion) were determined daily, from day 1 to day 8 of culture. The compounds dose inhibition cell proliferations by 50% (IC_{50}) were calculated at days 5 and 7 of treatment.

RNA Extraction. For RNA extraction, about 5×10^5 Hep G2 cells were seeded in 6-well plates, and at 24 h after plating, derivatives **c** and **i** were diluted in the medium to the concentration, as noted in Figure 11. Cells were washed once with PBS, and new medium containing the derivative was added directly to the flask. About 1×10^5 CA46 and Ramos cells were seeded in 6-well plates, and derivatives **c** and **i** were diluted in medium to 10 μM and added to the flask. Cells were harvested 24 h after initial treatment concurrently with untreated cells. Cell pellets were lysed in Redzol solution from the Total RNA Isolation Kit. RNA was extracted according to the protocol included with the kit and eluted in distilled, deionized water with 0.1% diethyl pyrocarbonate (DEPC) to a final

volume of 50 μL. RNA was quantitated spectrophotometrically and stored at −80 °C.

RT-PCR. Total RNA was used as a template for reverse transcription using the following protocol: each 20-μL reaction contained 1×M-MLV buffer, 500 μM dNTP, 100 pmol oligo dT primer, 100 units of M-MLV reverse transcriptase, DEPC in water (DEPC−H_2O), and 1 μg of total RNA. Mixtures were incubated at 42 °C for 60 min for reverse transcription and then at 92 °C for 10 min to inactivate the enzyme. PCR was performed according to the following protocol: each 20-μL reaction contained 1×PCR buffer, 500 μM dNTPs, 0.15 μM *β-actin* primers, 1.5 μM *c-myc* primers, 1 unit of *Taq* polymerase, 0.1% DEPC−H_2O, and 3 μL of the cDNA template. The reactions were incubated in a DNA Engine Peltier Thermal Cycler as follows: 95 °C for 5 min, followed by 36 cycles of 95 °C for 1 min, 50 °C for 1 min, and 72 °C for 1 min. The amplified products were separated on a 1.5% agarose gel, and photos were taken on a Gel Doc 2000 Imager System.

Molecular Modeling. The initial models of loop isomers A and B were built upon the X-ray structure of human telomeric sequence d[AGGG-(TTAGGG)3] from Protein Data Bank (1KF1).[24] The structure was then imported into Insight II package (Accelrys Inc., San Diego, CA),[28] and necessary modifications were carried out including replacements and deletions of bases. Missing loop nucleotides were added using single-strand B-DNA geometry using the Biopolymer module. Two potassium ions were placed between the G-tetrad planes to stabilize the tetrad structure. The initial models were then immersed in a box of TIP3P water molecules,[29] and an appropriate number of sodium ions was added to neutralize the negative charge of the phosphate backbone. The molecular dynamics simulations were carried out in NAMD[30] with VMD[31] monitoring the process. The CHARMM force field[32] parameter was assigned to every atom, and the Particle Mesh Ewald electrostatics[33] was used to compute long-range electrostatic interactions. Hydrogen atoms were added and minimized by 3000 steps of conjugate gradient minimization. After 4000 steps of conjugate gradient minimization, two stages of molecular dynamics simulations were carried out at 300 K. In the first stage, only the loop area atoms were allowed to move, and this process involved a 20 ps equilibration and 100 ps simulations. The second stage involved unrestrained molecular dynamics simulations with 20 ps equilibration and 100 ps simulations at 300 K. Trajectories were recorded every 0.1 ps, and the most stable structure was extracted and further refined by 2500 steps of conjugate gradient minimization.

Molecular docking was performed using the ICM-Pro 3.4-8a program (Molsoft).[22] According to the ICM method, the molecular system was described using internal coordinates as variables. The biased probability Monte Carlo (BPMC) minimization procedure was used for global energy optimization. The BPMC global energy optimization method consists of the following steps: (1) a random conformation change of the free variables according to a predefined continuous probability distribution; (2) a local energy minimization of analytical differentiable terms; (3) a calculation of the complete energy including nondifferentiable terms such us entropy and solvation energy; and (4) an acceptance or rejection of the total energy based on the Metropolis criterion and return to step 1. The binding between **i** or **c** and DNA molecules (Pu18A and Pu18B) was evaluated by binding energy, where the energy reflected the quality of the complex and included grid energy, continuum electrostatic, and entropy terms. In the docking analysis, the binding site was assigned across the entire structure of the DNA molecule. ICM docking was performed to find the most favorable orientation. The resulting **i**/**c**−DNA complex trajectories were energy minimized, and the interaction energies were computed.

Acknowledgment. We thank the Natural Science Foundation of China (Grant 20472117), the NSFC/RGC Joint Research Scheme (Grants 20710006, N_PolyU 508/06), the Science Foundation of Zhuhai (Grant PC20041131), the Science Foundation of Guangzhou (2006Z2-E402), the State Education Ministry, the Shenzhen Key Laboratory Fund, the University Grants Committee Areas of Excellence Scheme in Hong Kong (Grant AoE P/10-01), and the Hong Kong Polytechnic University Area of Strategic Development Fund for financial support of this study. The authors are grateful to Prof. An-long Xu of School of Life Science, Sun Yat-sen University, for providing the facilities for this work. And we thank Dr. Jun-min Quan from the Graduate School of Peking University for his self-giving technical support for our work.

Supporting Information Available: CD spectra and CD melting profiles of Pu27 with **a**−**e** and **g**−**j**, Pu27-11,20 with **c** and **i**, Pu27-11,23 with **c** and **i**, Pu27-14,20 with **c** and **i**, and Pu27-14,23 with **c** and **i**, and Job plot. This material is available free of charge via the Internet at http://pubs.acs.org.

References

(1) Resar, L. M.; Emison, E.; Kim, S.; Li, Q.; Prescott, J. E.; Wonsey, D.; Zeller, K. Function of the c-Myc oncogenic transcription factor. *Exp. Cell Res.* **1999**, *253*, 63−77.
(2) Simonsson, T.; Pribylova, M.; Vorlickova, M. A nuclease hypersensitive element in the human c-myc promoter adopts several distinct i-tetraplex structures. *Biochem. Biophys. Res. Commun.* **2000**, *278*, 158−166.
(3) Postel, E. H.; Berberich, S. J.; Rooney, J. W.; Kaetzel, D. M. Human NM23/nucleoside diphosphate kinase regulates gene expression through DNA binding to nuclease-hypersensitive transcriptional elements. *J. Bioenerg. Biomembr.* **2000**, *32*, 277−284.
(4) Simonsson, T.; Pecinka, P.; Kubista, M. DNA tetraplex formation in the control region of c-myc. *Nucleic Acids Res.* **1998**, *26*, 1167−1172.
(5) Michelotti, E. F.; Tomonaga, T.; Krutzsch, H.; Levens, D. Cellular nucleic acid binding protein regulates the CT element of the human c-myc protooncogene. *J. Biol. Chem.* **1995**, *270*, 9494−9499.
(6) Tomonaga, T.; Levens, D. Activating transcription from single stranded DNA. *Proc. Natl. Acad. Sci. U.S.A.* **1996**, *93*, 5830−5835.
(7) Siddiqui-Jain, A.; Grand, C. L.; Bearss, D. J.; Hurley, L. H. Direct evidence for a G-quadruplex in a promoter region and its targeting with a small molecule to repress c-MYC transcription. *Proc. Natl. Acad. Sci. U.S.A.* **2002**, *99*, 11593−11598.
(8) Lemarteleur, T.; Gomez, D.; Paterski, R.; Mandine, E.; Mailliet, P.; Riou, J. F. Stabilization of the c-myc gene promoter quadruplex by specific ligands' inhibitors of telomerase. *Biochem. Biophys. Res. Commun.* **2004**, *323*, 802−808.
(9) Grand, C. L.; Han, H.; Munoz, R. M.; Weitman, S.; Von Hoff, D. D.; Hurley, L. H.; Bearss, D. J. The cationic porphyrin TMPyP4 down-regulates c-MYC and human telomerase reverse transcriptase expression and inhibits tumor growth in vivo. *Mol. Cancer Ther.* **2002**, *1*, 565−573.
(10) Seenisamy, J.; Bashyam, S.; Gokhale, V.; Vankayalapati, H.; Sun, D.; Siddiqui-Jain, A.; Streiner, N.; Shin-ya, K.; White, E.; Wilson, W. D.; Hurley, L. H. Design and synthesis of an expanded porphyrin that has selectivity for the c-MYC G-quadruplex structure. *J. Am. Chem. Soc.* **2005**, *127*, 2944−2959.
(11) (a) Guittat, L.; Alberti, P.; Rosu, F.; Miert, S.V.; Thetiot, E.; Pieters, L.; Gabelica, V.; Pauw, E. D.; Ottaviani, A.; Riou, J.-F.; Mergny, J.-L. Interactions of cryptolepine and neocryptolepine with unusual DNA structures. *Biochimie* **2003**, *85*, 535−547. (b) Zhou, J. L.; Lu, Y. J.; Ou, T. M.; Zhou, J. M.; Huang, Z. S.; Zhu, X. F.; Du, C. J.; Bu, X. Z.; Ma, L.; Gu, L. Q.; Li, Y. M.; Chan, S. C. Synthesis and evaluation of quindoline derivatives as G-quadruplex inducing and stabilizing ligands and potential inhibitors of telomerase. *J. Med. Chem.* **2005**, *48*, 7315−7321.
(12) Zhou, J. M.; Zhu, X. F.; Lu, Y. J.; Deng, R.; Huang, Z. S.; Mei, Y. P.; Wang, Y.; Huang, W. L.; Liu, Z. C.; Gu, L. Q.; Zeng, Y. X. Senescence and telomere shortening induced by novel potent G-quadruplex interactive agents, quindoline derivatives, in human cancer cell lines. *Oncogene* **2006**, *25*, 503−511.
(13) Balagurumoorthy, P.; Brahmachari, S. K. Structure and stability of human telomeric sequence. *J. Biol. Chem.* **1994**, *269*, 21858−21869.
(14) Balagurumoorthy, P.; Brahmachari, S. K.; Mohanty, D.; Bansal, M.; Sasisekharan, V. Hairpin and parallel quadruplex structures for telomeric sequences. *Nucleic Acids Res.* **1992**, *20*, 4061−4067.
(15) Seenisamy, J.; Rezler, E. M.; Powell, T. J.; Tye, D.; Gokhale, V.; Joshi, C. S.; Siddiqui-Jain, A.; Hurley, L. H. The dynamic character of the G-quadruplex element in the c-MYC promoter and modification by TMPyP4. *J. Am. Chem. Soc.* **2004**, *126*, 8702−8709.

(16) Kim, M. Y.; Gleason-Guzman, M.; Izbicka, E.; Nishioka, D.; Hurley, L. H. The different biological effects of telomestatin and TMPyP4 can be attributed to their selectivity for interaction with intramolecular or intermolecular G-quadruplex structures. *Cancer Res*. **2003**, *63*, 3247−3256.
(17) Ren, J.; Chaires, J. B. Sequence and structural selectivity of nucleic acid binding ligands. *Biochemistry* **1999**, *38*, 16067−16075.
(18) (a) Rossetti, L.; Franceschin, M.; Bianco, A.; Ortaggi, G.; Savino, M. Perylene diimides with different side chains are selective in inducing different G-quadruplex DNA structures and in inhibiting telomerase. *Bioorg. Med. Chem. Lett*. **2002**, *12*, 2527−2533. (b) Wheelhouse, R. T.; Jennings, S. A.; Philips, V. A.; Pletsas, D.; Murphy, P. M.; Garbett, N. C.; Chaires, J. B.; Jenkins, T. C. Design, synthesis, and evaluation of novel biarylpyrimidines: A new class of ligand for unusual nucleic acid structures. *J. Med. Chem*. **2006**, *49*, 5187−5198.
(19) Facchini, L. M.; Penn, L. Z. The molecular role of Myc in growth and transformation: Recent discoveries lead to new insight. *FASEB J*. **1998**, *12*, 633−651.
(20) Simonsson, T.; Henriksson, M. C-myc suppression in Burkitt's lymphoma cells. *Biochem. Biophys. Res. Commun*. **2002**, *290*, 11−15.
(21) (a) Wheelhouse, R. T.; Sun, D.; Han, H.; Han, F. X.; Hurley, L. H. Cationic porphyrins as telomerase inhibitors: the interaction of tetra-(*N*-methyl-4-pyridyl)porphine with quadruplex DNA. *J. Am. Chem. Soc*. **1998**, *120*, 3261−3262. (b) Likussar, W.; Blotz, D. F. Theory of continuous variations plots and a new method for spectrophotoetric determination of extraction and formation constants. *Anal. Chem*. **1971**, *43*, 1265−1272.
(22) Totrov, M.; Abagyan, R. Flexible protein−ligand docking by global energy optimization in internal coordinates. *Proteins* **1997**, *1* (Suppl.), 215−220.
(23) Harrison, R. J.; Cuesta, J.; Chessari, G.; Read, M. A.; Basra, S. K.; Reszka, A. P.; Morrell, J.; Gowan, S. M.; Incles, C. M.; Tanious, F. A.; Wilson, W. D.; Kelland, L. R.; Neidle, S. Trisubstituted acridine derivatives as potent and selective telomerase inhibitors. *J. Med. Chem.* **2003**, *46*, 4463−4476.
(24) Parkinson, G. N.; Lee, M. P. H.; Neidle, S. Crystal structure of parallel quadruplexes from human telomeric DNA. *Nature* **2002**, *417*, 876−880.
(25) DeLano, W. L. *The PyMOL Molecular Graphics System*; DeLano Scientific: San Carlos, CA.
(26) Ambrus, A.; Chen, D.; Dai, J. X.; Jones, R. A.; Yang, D. Z. Solution structure of the biologically relevant G-quadruplex element in the human c-myc promoter. Implications for G-quadruplex stabilization. *Biochemistry* **2005**, *44*, 2048−2058.
(27) Ruan, F.; Liu, S. Y. Combination antigene therapy targeting c-myc and c-erbB2 in the ovarian cancer COC1 cell line. *Gynecol. Oncol.* **2002**, *85*, 40−44.
(28) *Insight II*; molecular modeling software; Accelrys Inc.: 9685 Scranton Rd., San Diego, CA, 92121, 2000.
(29) Jorgensen, W. L.; Chandresekhar, J.; Madura, J. D.; Impey, R. W.; Klein, M. L. Comparison of simple potential functions for simulating liquid water. *J. Chem. Phys.* **1983**, *79*, 926−935.
(30) Kale, L.; Skeel, R.; Bhandarkar, M.; Brunner, R.; Gursoy, A.; Krawetz, N.; Phillips, J.; Shinozaki, A.; Varadarajan, K.; Schulten, K. NAMD2: Greater scalability for parallel molecular dynamics. *J. Comput. Phys.* **1999**, *151*, 283−312.
(31) Humphrey, W.; Dalke, A.; Schulten, K. VMD: Visual molecular dynamics. *J. Mol. Graphics* **1996**, *14*, 33−38, 27−28.
(32) MacKerell, A. D., Jr.; Bashford, D.; Bellott, M.; Dunbrack, R. L., Jr.; Evanseck, J.; Field, M. J.; Fischer, S.; Gao, J.; Guo, H.; Ha, S.; Joseph, D.; Kuchnir, L.; Kuczera, K.; Lau, F. T. K.; Mattos, C.; Michnick, S.; Ngo, T.; Nguyen, D. T.; Prodhom, B.; Reiher, I. W. E.; Roux, B.; Schlenkrich, M.; Smith, J.; Stote, R.; Straub, J.; Watanabe, M.; Wiorkiewicz−Kuczera, J.; Yin, D.; Karplus, M. All-atom empirical potential for molecular modeling and dynamics study of proteins. *J. Phys. Chem. B.* **1998**, *102*, 3586−3616.
(33) Darden, T.; York, D.; Pedersen, L. Particle mesh ewald: An N.log-(N) method for ewaid sums in large systems. *J. Chem. Phys.* **1993**, *98*, 10089−10092.

JM0610088